Supplementary Information for Inelastic resonant tunnelling through adjacent localised electronic states in van der Waals heterostructures

E. E. Vdovin[1], K. Kapralov[2], Yu. N. Khanin[1], A. Margaryan[3], K. Watanabe[4], T. Taniguchi[4], C. Yang[5], S. V. Morozov[1], D. A. Svintsov[2], K. S. Novoselov[6, *] and D. A. Ghazaryan[3, 6, *]

[1]Institute of Microelectronics Technology RAS, Chernogolovka, 142432, Russia

[2]Center for Photonics and 2D Materials, Moscow Institute of Physics and Technology, Dolgoprudny, 141701, Russia

[3]Laboratory of Advanced Functional Materials, Yerevan State University, Yerevan, 0025, Republic of Armenia

[4]National Institute for Materials Science, Namiki 1-1, Tsukuba 305-0044, Ibaraki, Japan

[5]State Key Laboratory of Physical Chemistry of Solid Surfaces, Collaborative Innovation Center of Chemistry for Energy Materials (iChEM), College of Chemistry and Chemical Engineering, Xiamen University, Xiamen, 361005, China

[6]Institute for Functional Intelligent Materials, National University of Singapore, Singapore, 117575, Republic of Singapore

*Correspondence should be addressed to davitghazaryan@ysu.am and kostya@nus.edu.sg

Supplementary Note 1: Theoretical evaluation of inelastic tunnelling current probability through adjacent localised electronic states in *h*BN barrier

Supplementary Note 2: Device schematics: dual gated Gr-*h*BN-BGr

Supplementary Note 3: Electrostatic model for resonant features arising from other localised electronic states in *h*BN Barrier, Gr-*h*BN-BGr, Device 1

Supplementary Note 4: Relative shift of localised electronic states A and B in *h*BN barrier along their conductive channels at fixed V_{tg} = 3 V, Gr-*h*BN-BGr, Device 1

Supplementary Note 5: Resonant tunnelling through adjacent localised electronic states in *h*BN barrier, Gr-*h*BN-BGr, Device 2

Supplementary Note 6: The dependence of fine-features on the applied top gate voltage extracted through the spectroscopy by localised electronic states in *h*BN, Gr-*h*BN-BGr, Device 1

Supplementary Note 7: Resonant inelastic tunnelling as a tool for the spectroscopy of delicate features in electronic density of states of electrode layers, perpendicular magnetic fields, Gr-*h*BN-BGr, Device 1

Supplementary Note 1: Theoretical evaluation of inelastic tunnelling current probability through adjacent localised electronic states in *h*BN barrier

Rate equation approach to the elastic and inelastic tunnelling events. We proceed to the derivation of the conditions when the inelastic tunnelling current between two localised electronic states can be stronger than elastic current through the individual states. We consider a scheme as in Supplementary Figure 1 with localised electronic states labelled as A and B. An electron on A^{th} localised electronic state may choose either the long elastic path or the short inelastic path. Therefore, for dominance of inelastic current, the inelastic coupling constant $|g^2|$ should be larger than the tunnel exponent of the path difference of $\exp(-2\kappa\Delta L)$.

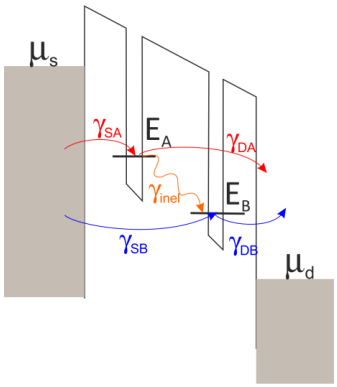

Supplementary Figure 1. Band diagram of the two-localised state system along with possible hopping rates.

We introduce hopping amplitudes of

$$\gamma_{ij} = \gamma_{el}^{(0)}\, exp\big(-2\kappa|L_{ij}|\big), \tag{1.1}$$

where i and j describe the source, drain, and positions of A^{th} and B^{th} localised electronic states. The source and drain graphene layers have distribution functions of f_S *and* f_D. The inelastic tunnelling rate can be presented as

$$\gamma_{inel} = \gamma_{inel}^{(0)}\exp(-2\kappa|L_{AB}|), \tag{1.2}$$

where $\gamma_{inel}^{(0)}$ is the coupling constant to elementary excitations, for example, phonons or plasmons. It has the dimension of energy. It is also convenient to introduce the dimensionless coupling constant of

$$|g|^2 = \frac{\gamma_{inel}^{(0)}}{\gamma_{el}^{(0)}}. \tag{1.3}$$

The populations of localised electronic states of f_A and f_B are found from the detailed balance:

$$\begin{aligned}\frac{df_A}{dt} &= \gamma_{SA}(f_S - f_A) + \gamma_{DA}(f_D - f_A) - \gamma_{inel}f_A(1 - f_B),\\ \frac{df_B}{dt} &= \gamma_{SB}(f_S - f_B) + \gamma_{DB}(f_D - f_B) + \gamma_{inel}f_A(1 - f_B).\end{aligned} \tag{1.4}$$

Note, that there is no Pauli principle for elastic tunnelling events[1], but there is one for inelastic events. We assume $T = 0$ K, so only inelastic emission is possible, no absorption. At finite T, a replacement should be made as

$$\gamma_{inel}f_A(1 - f_B) \to \gamma_{inel}\{f_A(1 - f_B)[N_B(\omega_{AB}) + 1] - f_B(1 - f_A)N_B(\omega_{AB})\}. \tag{1.5}$$

Though steady-state populations of $f_{A,B}$ can be found fully analytically, here, we first find an approximate solution neglecting the inelastic term γ_{inel}. Those populations are:

$$f_A = \frac{\gamma_{SA}}{\gamma_{SA}+\gamma_{DA}} f_S + \frac{\gamma_{DA}}{\gamma_{SA}+\gamma_{DA}} f_D \approx \frac{\gamma_{SA}}{\gamma_{SA}+\gamma_{DA}} f_S \approx f_S \tag{1.6}$$

In the first step, we assume zero temperature and large bias $f_D \to 0$. In the second step, for the first localised electronic state, we assume that the source-localised state path is shorter than the drain-localised state link $\gamma_{SA} \gg \gamma_{DA}$. Similar line of arguments is made for the second localised electronic state:

$$f_B = \frac{\gamma_{SB}}{\gamma_{SB}+\gamma_{DB}} f_S + \frac{\gamma_{DB}}{\gamma_{SB}+\gamma_{DB}} f_D \approx \frac{\gamma_{SB}}{\gamma_{SB}+\gamma_{DB}} f_S \approx \frac{\gamma_{SB}}{\gamma_{DB}} f_S \ll 1 \tag{1.7}$$

The elastic current is again computed from the detailed balance:

$$I_{el} = \gamma_{SA}(f_S - f_A) + \gamma_{SB}(f_S - f_B) = \left(\frac{\gamma_{SA}\gamma_{DA}}{\gamma_{SA}+\gamma_{DA}} + \frac{\gamma_{SB}\gamma_{DB}}{\gamma_{SB}+\gamma_{DB}}\right)(f_S - f_D) \tag{1.8}$$

We now use the relations between hopping amplitudes:

$$I_{el} \approx (\gamma_{DA} + \gamma_{SB})(f_S - f_D) \tag{1.9}$$

Considering that the current is proportional to the permeability of the strongest link. This contrasts with a simple intuition that the product of permeabilities should be there $I_{el} \neq (\gamma_{DA}\gamma_{SA} + \gamma_{SB}\gamma_{DB})(f_S - f_D)$. The reason is that localised states A and B are already populated almost exactly as the source and the drain electrodes. Plugging the populations (1.6) and (1.7) into the rate equation of inelastic processes, we get:

$$I_{inel} = \gamma_{inel} f_A (1 - f_B) = \gamma_{inel} \frac{\gamma_{SA}}{\gamma_{SA}+\gamma_{DA}} f_S \left(1 - \frac{\gamma_{SB}}{\gamma_{SB}+\gamma_{DB}} f_S\right) \approx \gamma_{inel} f_S. \tag{1.10}$$

The dominance of inelastic current (2.10) over elastic one (2.9) appears, when:

$$\gamma_{inel} > \gamma_{DA} + \gamma_{SB} \tag{1.11}$$

Plugging the explicit exponentials (1.1) and (1.2), we find another form of criteria:

$$\frac{\gamma_{inel}^{(0)}}{\gamma_{el}^{(0)}} > exp[-2\kappa L_{SA}] + exp[-2\kappa L_{DB}] \tag{1.12}$$

In the simplest case of equidistant localised electronic states of $L_{SA} = L/3 = L_{DB}$ (L is the *h*BN barrier thickness), this simplifies to:

$$\frac{\gamma_{inel}^{(0)}}{\gamma_{el}^{(0)}} > 2\, exp\left[-\frac{2}{3}\kappa L\right] \tag{1.13}$$

The above criteria of dominance of inelastic tunnelling, (1.12) and (1.13), can be understood in the following way. The left-hand side of these expressions is the non-exponential function of distance between localised electronic states and graphene electrodes, it is proportional to the coupling strength between electrons and elementary excitations. The right-hand side exponentially decays as we increase the distance between impurities and graphene layers. Thus, for large distances of L_{SA} and L_{DB}, the inelastic tunnelling will always be dominant.

Finally, solving the full nonlinear balance equation model for two equidistant localised electronic states confirms the approximations above as it is shown in the Supplementary Figure 2.

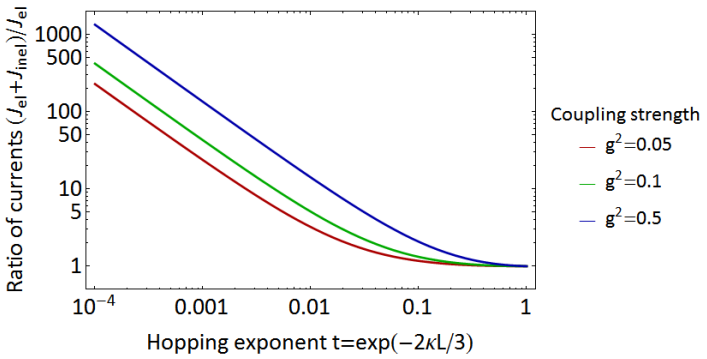

Supplementary Figure 2. Ratio of full current to elastic current *vs* the transparency of the one-third section of the tunnelling barrier. Results are shown for three different inelastic coupling constants. The inelastic events become dominant when the transparency is low and coupling constant is large.

Estimates of rates for the elastic and inelastic tunneling events. The elastic tunneling rate is of the order of "beating frequency" of electron in a potential of a localized electronic state, *i. e.*:

$$\gamma_{el}^{(0)} \approx \frac{\Delta}{\hbar}, \tag{1.14}$$

where $\Delta \approx 1.5$ eV is the barrier height in between the neutrality point in graphene electrode and the band bottom in *h*BN. The inelastic tunneling rate associated with transfer of energy to individual electron-hole pairs in graphene (Auger effect) is:

$$\gamma_{inel}^{(0)} = \frac{9\pi^5}{256}\frac{\varepsilon_F}{\hbar}\alpha_C^2(\kappa z_{AB})^3, \tag{1.15}$$

where $\alpha_C = e^2/\varepsilon\hbar v_0 = 300/(4\times 137)$ is the coupling constant for Coulomb interactions, ε_F is the Fermi energy in individual graphene layer, κ is the decay rate of the wave function of localized electronic state, z_{AB} is the distance between localized electronic states. The decay constant under the barrier can be estimated from layer-dependent resistance[2]:

$$\kappa = -\frac{1}{2}\frac{d\ln R}{dL} = 5.8\times 10^9\ \mathrm{m}^{-1}. \tag{1.16}$$

Further numerical estimate results in:

$$|g|^2 = \frac{\gamma_{inel}^{(0)}}{\gamma_{el}^{(0)}} = \frac{9\pi^3}{1024}\frac{\varepsilon_F}{\Delta}\alpha_C^2(\kappa z_{AB})^3 \approx 0.27\times\frac{0.1\ \mathrm{eV}}{1.5\ \mathrm{eV}}\times 0.55^2(5.8\ \mathrm{nm}^{-1}\times 0.66\ \mathrm{nm})^2 \sim 0.3. \tag{1.17}$$

It implies that Coulomb interactions resulting in an Auger effect are not weak at all, the dimensionless coupling strength is just slightly less than unity. On the other hand, the combination of tunneling exponents can be estimated as:

$$exp[-2\kappa L_{SA}] + exp[-2\kappa L_{DB}] \sim 5\times 10^{-4}, \tag{1.18}$$

which is fulfilling the criteria of dominance of inelastic tunneling events. Now we pass to realistic estimates of γ_{inel} associated with Auger process, *i. e.*, excitation of individual electrons in layers upon hopping of another electron between localized electronic states. Here, the Fermi Golden Rule number of transition events in unit time can be written as:

$$\frac{df_A}{dt} = \sum_{p,q} W_{e-e} f_A(1-f_B)f_p\left(1-f_{p-q}\right), \tag{1.19}$$

where $f_{A,B}$ are the distribution functions of localized electronic states, $f_{p,p-q}$ are the distribution functions of layer electrons, and the scattering probability in unit time is:

$$W_{e-e} = \frac{2\pi}{\hbar}|\langle p, A|V_{coul}|p+q, B\rangle|^2 \delta\left(\varepsilon_{p+q} - \left(\varepsilon_{p-q} - E_{AB}\right)\right). \quad (1.20)$$

At this stage, we introduce the polarizability function as:

$$\frac{df_A}{dt} = \frac{2A}{\hbar} f_A(1-f_B)[N(\omega_{AB})+1]\sum_q |\langle p, A|V_{coul}|p+q, B\rangle|^2 \, Im\, \Pi(q, \omega_{AB}). \quad (1.21)$$

The rate equations (1.4) and (1.5) are now microscopically justified, with inelastic scattering rate given by:

$$\gamma_{inel} = \frac{2A}{\hbar}\sum_q |\langle p, A|V_{coul}|p+q, B\rangle|^2 \, Im\, \Pi(q, \omega_{AB}). \quad (1.22)$$

The matrix element is evaluated for Coulomb interaction operator between two-particle states. One is localized at the localized electronic state and the other one is a plane wave at the graphene layer. In explicit form, it can be introduced as:

$$\langle p, A|V_{coul}|p+q, B\rangle = \int \frac{dr_1}{A} dr_2 e^{-ipr_2}\psi_A(r_1)\frac{e^2}{|r_1-r_2|}e^{-i(p+q)r_2}\psi_B(r_1). \quad (1.23)$$

Let us transform these expressions to computationally efficient forms.

$$\langle p, A|V_{coul}|p+q, B\rangle = \frac{1}{Av}\frac{2\pi e^2}{|q|}\int dz_1 d\rho_1 \, exp(-|q|z_1 + iq\rho_1)\, exp\left(-\kappa\sqrt{\rho_1^1 + (z_1 - z_A)^2} - \kappa\sqrt{\rho_1^1 + (z_1 - z_B)^2}\right), \quad (1.24)$$

where $\nu = \pi/\kappa^3$ is the normalization factor of hydrogen-like wave function. Integrating over in-plane angles, we get:

$$\langle p, A|V_{coul}|p+q, B\rangle = \frac{1}{A}\frac{4\pi e^2\kappa^3}{|q|} I$$
$$I = \int dz_1 \rho_1 d\rho_1 J_0(q\rho_1)\, exp\left(-\kappa\sqrt{\rho_1^2 + (z_1 - z_A)^2} - \kappa\sqrt{\rho_1^2 + (z_1 - z_B)^2} - qz_1\right). \quad (1.25)$$

We reckon the z-coordinate from the center of localized electronic states $z_1 = \xi + (z_A + z_B)/2 \cong \xi + \bar{z}$, and the expression becomes:

$$I = \int d\xi \rho_1 d\rho_1 J_0(q\rho_1)\, exp\left(-\kappa\sqrt{\rho_1^1 + \left(\xi - \frac{z_{AB}}{2}\right)^2} - \kappa\sqrt{\rho_1^1 + \left(z_1 + \frac{z_{AB}}{2}\right)^2} - q(\xi + \bar{z})\right). \quad (1.26)$$

Introducing elliptic coordinates, we get:

$$I = e^{-q\bar{z}}\left(\frac{z_{AB}}{2}\right)^3 \int dudv(u^2 - v^2)\sqrt{1-v^2}\sqrt{u^2-1} J_0\left(\frac{qz_{AB}}{2}\sqrt{u^2-1}\sqrt{1-v^2}\right) exp\left(-\left(\kappa + \frac{qv}{2}\right)z_{AB}u\right). \quad (1.27)$$

In new variables of $Q = qz_{AB}/2$, $\varkappa = \kappa z_{AB}$, we get a simple two-parametric function of:

$$I = e^{-q\bar{z}}\left(\frac{z_{AB}}{2}\right)^3 \int dudv(u^2 - v^2)\sqrt{u^2-1}\sqrt{1-v^2} J_0\left(Q\sqrt{u^2-1}\sqrt{1-v^2}\right) exp(-(\varkappa + Qv)u). \quad (1.28)$$

For $\varkappa >> Q$, we proceed with steepest descend:

$$I = e^{-q\bar{z}}\left(\frac{z_{AB}}{2}\right)^3 \int dudv(u^2 - v^2)\sqrt{u^2-1}\sqrt{1-v^2} J_0\left(Q\sqrt{u^2-1}\sqrt{1-v^2}\right) exp(-(\varkappa + Qv)u) \approx$$

$$\approx e^{-q\bar{z}}\left(\frac{Z_{AB}}{2}\right)^3\sqrt{2}\int_{-1}^{1}dv(1-v^2)^{3/2}\int_{1}^{\infty}du\sqrt{u-1}\,exp(-(\varkappa+Qv)u)\approx$$

$$\approx e^{-q\bar{z}}\left(\frac{Z_{AB}}{2}\right)^3 e^{-\varkappa}\sqrt{\frac{\pi}{2}}\int_{-1}^{1}dv(1-v^2)^{3/2}\frac{e^{-Qv}}{(\varkappa+Qv)^{3/2}}\approx$$

$$\approx e^{-q\bar{z}}\left(\frac{z_{AB}}{2}\right)^3\frac{e^{-\varkappa}}{\varkappa^{3/2}}\sqrt{\frac{\pi}{2}}\frac{3\pi I_2(Q)}{Q^2}\approx\frac{3\pi^{3/2}}{8\sqrt{2}}e^{-q\bar{z}}\left(\frac{z_{AB}}{2}\right)^3\frac{e^{-\varkappa}}{\varkappa^{3/2}} \tag{1.29}$$

Going back to dimensional variables, we find:

$$\langle p,A|V_{coul}|p+q,B\rangle=\frac{1}{A}\frac{e^2}{|q|}\frac{3\pi^{5/2}}{16\sqrt{2}}(\kappa z_{AB})^{3/2}e^{-q\bar{z}}e^{-\kappa z_{AB}}. \tag{1.30}$$

Next, going back to an original formula (1.22), we find:

$$\gamma_{inel}=\frac{1}{\hbar A}\frac{9\pi^5}{256}(\kappa z_{AB})^3e^{-2\kappa z_{AB}}\sum_q\left[\frac{e^2}{|q|}e^{-q\bar{z}}\right]^2 Im\,\Pi\,(q,\omega_{AB}). \tag{1.31}$$

The exponential scaling of $\gamma_{inel}=\gamma_{inel}^{(0)}\exp(-2\kappa z_{AB})$ is now justified.

For $Im\Pi(q,\omega_{AB})$, we use a classical approximation of:

$$Im(q,\omega_{AB})\approx AD_0(\varepsilon_F)\frac{\hbar\omega_{AB}}{\sqrt{(\hbar q v_F)^2-(\hbar\omega_{AB})^2}}. \tag{1.32}$$

All in all, that results in:

$$\gamma_{inel}^{(0)}=\frac{D_0(\varepsilon_F)}{\hbar}\frac{9\pi^5}{256}(\kappa z_{AB})^3\int_{\omega_{AB}/v_F}^{+\infty}\frac{e^4}{(2\pi)^2}\frac{dq}{q}e^{-2q\bar{z}}\frac{\hbar\omega_{AB}}{\sqrt{(\hbar q v_F)^2-(\hbar\omega_{AB})^2}}=$$

$$=\frac{D_0(\varepsilon_F)}{\hbar}\frac{9\pi^3}{1028}(\kappa z_{AB})^3e^4\int_1^{+\infty}\frac{d\tau}{\tau}\frac{e^{-2q_{th}\bar{z}\tau}}{\sqrt{\tau^2-1}}, \tag{1.33}$$

where $q_{th}=\omega_{AB}/v_0$. The integral in (1.33) can be presented as:

$$\int_1^{+\infty}\frac{d\tau}{\tau}\frac{e^{-2q_{th}\bar{z}\tau}}{\sqrt{\tau^2-1}}\approx\begin{cases}\frac{\pi}{2}, q_{th}\bar{z}\ll 1\\ \frac{1}{2}\sqrt{\frac{\pi}{q_{th}\bar{z}}}exp(-2q_{th}\bar{z}), q_{th}\bar{z}\gg 1\end{cases}. \tag{1.34}$$

Plugging in an explicit expression for density of electronic states:

$$D_0(\varepsilon_F)=\frac{N\varepsilon_F}{2\pi\hbar^2v_0^2}, \tag{1.35}$$

we finally find expressions for the inelastic tunnelling rate and coupling constant:

$$\gamma_{inel}^{(0)}=\frac{\varepsilon_F}{\hbar}\frac{9\pi^2}{512}(\kappa z_{AB})^3\alpha_C^2\int_1^{+\infty}\frac{d\tau}{\tau}\frac{e^{-2q_{th}\bar{z}\tau}}{\sqrt{\tau^2-1}}\approx\frac{\varepsilon_F}{\hbar}\frac{9\pi^3}{1024}(\kappa z_{AB})^3\alpha_C^2, \tag{1.36}$$

$$|g|^2=\frac{\varepsilon_F}{U_0}\frac{9\pi^3}{1024}(\kappa z_{AB})^3\alpha_C^2. \tag{1.37}$$

Supplementary Note 2: Device schematics: dual gated Gr-*h*BN-BGr

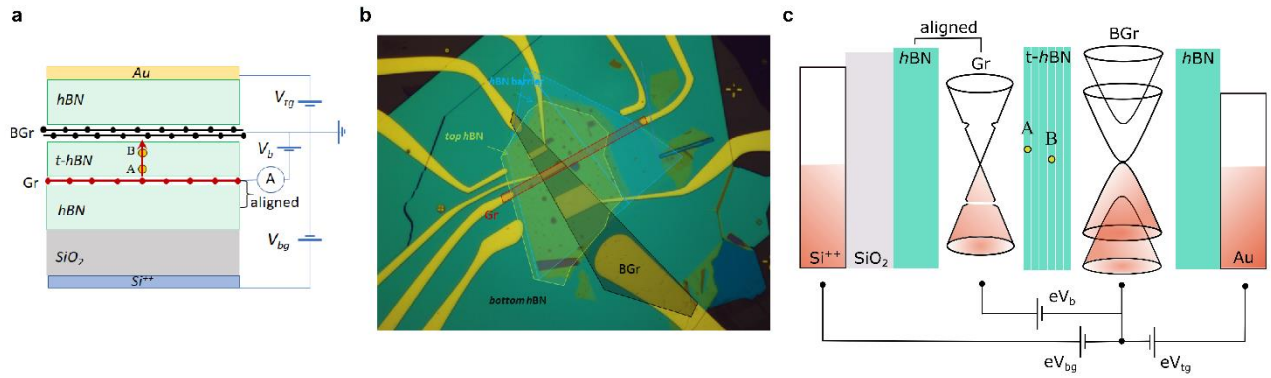

Supplementary Figure 3. The schematics (a), 50X optical micrograph (b) and band diagram illustration (c) of the device 1 under study. Monolayer and AB Bernal bilayer graphene electrodes are denoted as Gr and BGr. *h*BN stands for encapsulating and thick hexagonal boron nitride layers and t-*h*BN for tunnelling barrier. For the device 1, Gr was aligned with the bottom encapsulating *h*BN layer with a twist angle of about 1°, hence, the reconstructed band structure is introduced here. Si^{++}/SiO_2 denote the substrate, which was connected a back gate and Au stands for the top gate. Red shaded regions introduce the filled states at zero electric fields. A and B mark the zero electric field positions of the corresponding localised electronic states for device 1.

Supplementary Note 3: Electrostatic model for resonant features arising from other localised electronic states in *h*BN barrier, Gr-*h*BN-BGr, Device 1

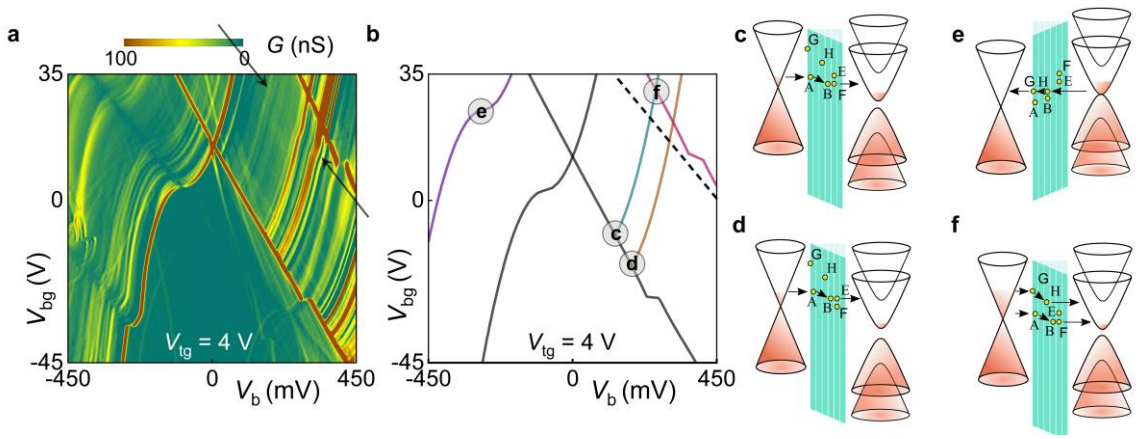

Supplementary Figure 4. The other localised electronic states in *h*BN barrier in device 1. **a,** Experimental differential tunnelling conductance maps at $T = 2$ K as a function of bias (V_b) and back gate (V_{bg}) voltages at fixed top gate voltages of $V_{tg} = 4$ V. Black arrows mark the distorted features in resonant tunnelling lines corresponding to the second e-side graphene neutrality point contribution to the tunnelling current. **b** Evaluated electrostatic lines corresponding to other elastic tunnelling events through a variety of electronic states E, F, G and H ($E_{0E} = 98$ meV, $E_{0F} = 90$ meV, $E_{0G} = 200$ meV, $E_{0H} = 130$ meV and $z_E = 5d/6$, $z_F = 5d/6$, $z_G = d/12$, $z_H = d/2$) energy as a function of back gate and bias voltages at fixed top gate voltages of $V_{tg} = 4$ V. The black dashed illustrates the position of the second e-side graphene neutrality point in the map. **c, d, h** and **f,** Illustrate the band diagrams corresponding to the events presented and marked in (b).

Supplementary Note 4: Relative shift of localised electronic states A and B in *h*BN barrier along their conductive channels at fixed V_{tg} = 3 V, Gr-*h*BN-BGr, Device 1

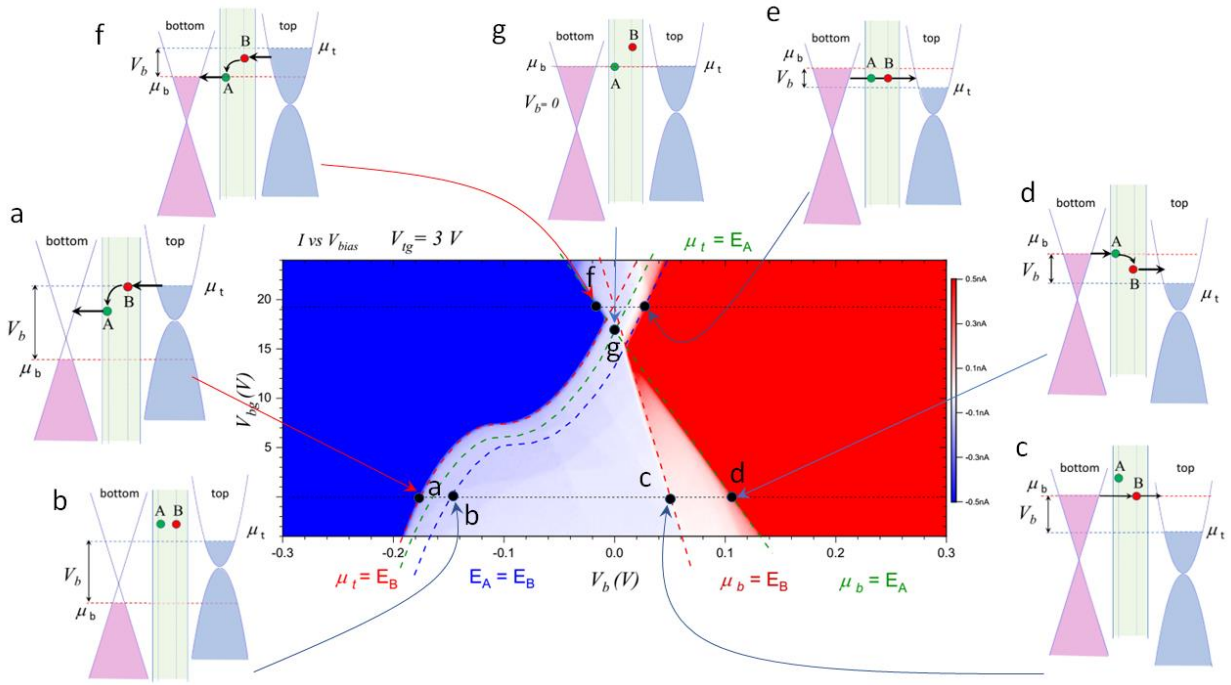

Supplementary Figure 5. The current-bias-backgate voltage contour map of the Device 1 at the fixed topgate voltage of V_{tg} = 3 V. Note that the inelastic resonant tunnelling channels emerge as steps in the current-voltage characteristics, and hence, appear as borderline resonances in the map. (a-c) Simplified schematic band diagrams illustrating the relative shift between the energy levels of localised electronic states A and B at various points all over the conductive channels. Here, $E_{A,B}$ are the energy levels of localised electronic states A and B, V_b is the bias voltage, $\mu_{t,b}$ are the chemical potentials of moiré monolayer and AB Bernal bilayer. The band diagrams of the latter two are simplified for clarity.

Supplementary Note 5: Resonant elastic tunnelling through adjacent localised electronic states in *h*BN barrier, Gr-*h*BN-BGr, Device 2

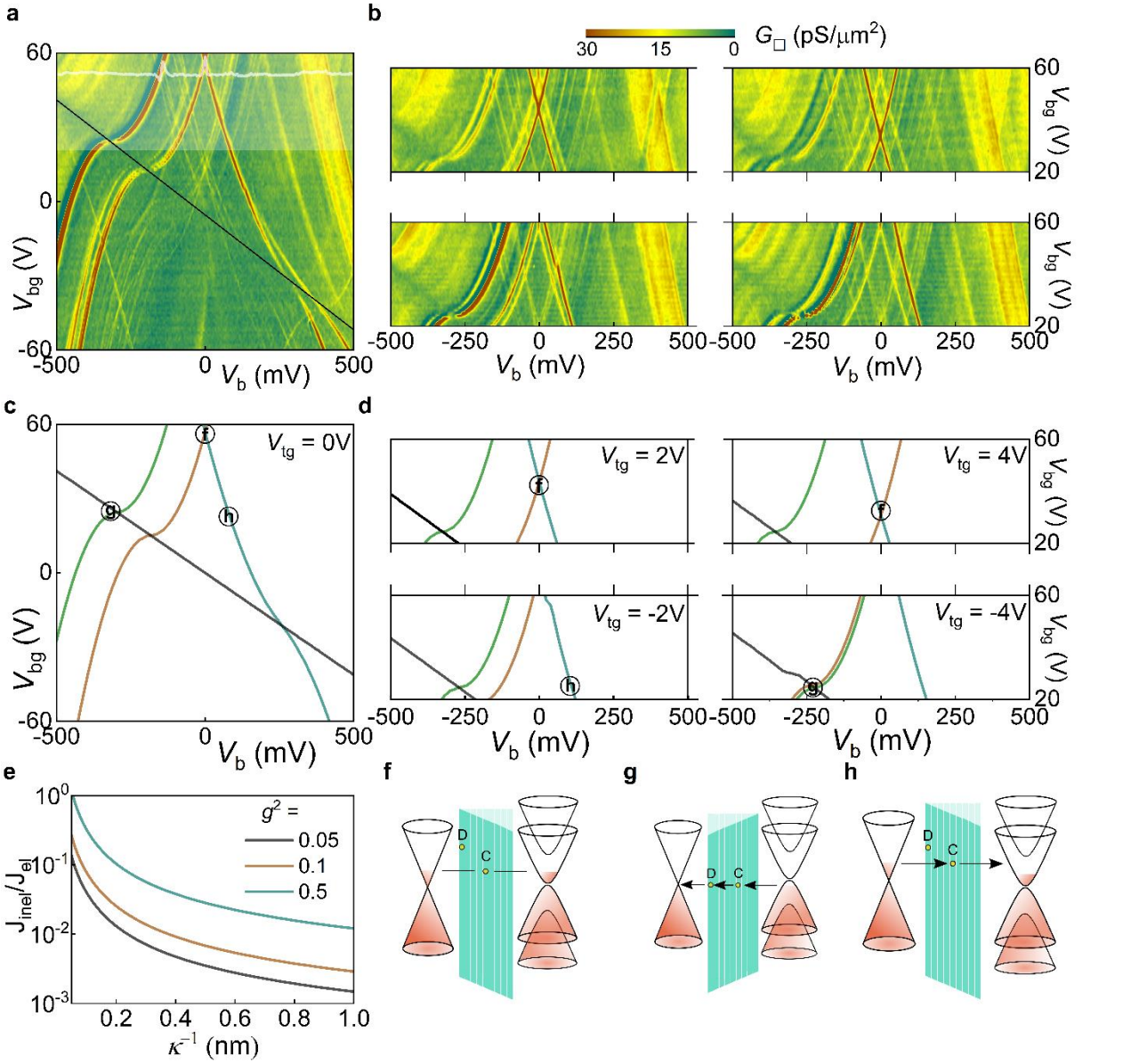

Supplementary Figure 6. The dominance of resonant elastic events for a tunnelling through two adjacent localised states their electric field tuning. **a** and **b,** Experimental differential tunnelling conductance maps at $T = 2$ K as a function of bias (V_b) and back gate (V_{bg}) voltages at fixed top gate voltages of $V_{tg} = 0$ V (a), $V_{tg} = 2, -2$ V (b) and $V_{tg} = 4, -4$ V (b). The tunnelling conductance values are normalized over the cross-sectional area of the device 2 ($S \approx 25$ μm^2). The white line represents the cut of the map presented in (a) at $V_{bg} = 57$ V. **c** and **d,** Evaluated electrostatic lines corresponding to both elastic and inelastic tunnelling events through states C and D (C and D) in series as a function of back gate and bias voltages at fixed top gate voltages of $V_{tg} = 0$ V (b), $V_{tg} = 2, -2$ V (e) and $V_{tg} = 4, -4$ V (h). Black lines in (a, c, d) illustrate the alignment of the chemical potential of monolayer graphene with its neutrality point. Here, the states C and D are located at $d/2$ and $d/18$ of the nine-layer thick *h*BN barrier (counting from the monolayer graphene, left electrode). Their energies at zero bias, back gate and top gate voltages are $E_{0C} = 107$ meV and $E_{0D} = 230$ meV. Evaluation of ratio of currents for inelastic to elastic tunnelling events for C to D for three coupling constants $|g|^2$ *vs* the length of the localization of a localised state, κ^{-1}. **f, g** and **h,** Illustrate the band diagrams corresponding to the events presented and marked in (c) and (d).

Supplementary Note 6: The dependence of fine-features on the applied top gate voltage extracted through the spectroscopy by localised electronic states in *h*BN, Gr-*h*BN-BGr, Device 1

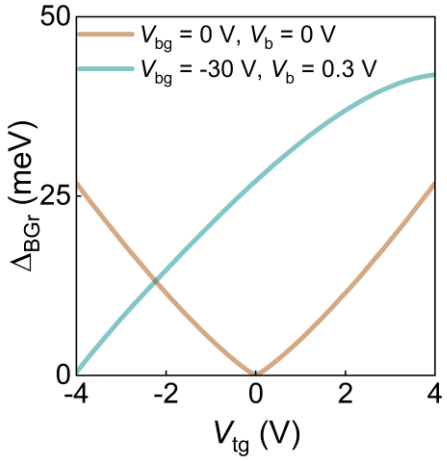

Supplementary Figure 7. Electric-field tuning of fine-features by the applied topgate voltage. The dependence of AB Bernal bilayer graphene's bandgap on the applied top gate voltage extracted from theoretical evaluations, which were initially fitted to the experimental results measured with a step of V_{tg} = 1 V. The bandgap extraction was done for a theoretical model with optimized parameters corresponding to the conductivity maps in Figure 2 of the main text of the paper as the bandgap of the band diagram of bilayer graphene at given values of V_b, V_{bg} и V_{tg}. It is important to note that the V_b gap length of the resonance line in Figure 3e of the main text is not exactly equal to the bandgap value. The resonant line in Figure 3e of the main text corresponds to the alignment of the Fermi level of monolayer graphene and localised electronic state A, and the line break is associated with getting this alignment in the forbidden zone of bilayer graphene. The position of this alignment line depends on V_b, V_{bg} and V_{tg} in a complex way, so the corresponding gap on V_b is not equal to the value of bandgap.

Supplementary Note 7: Resonant inelastic tunnelling as a tool for the spectroscopy of delicate features in electronic density of states of electrode layers, the case of perpendicular magnetic fields, Gr-*h*BN-BGr, Device 1

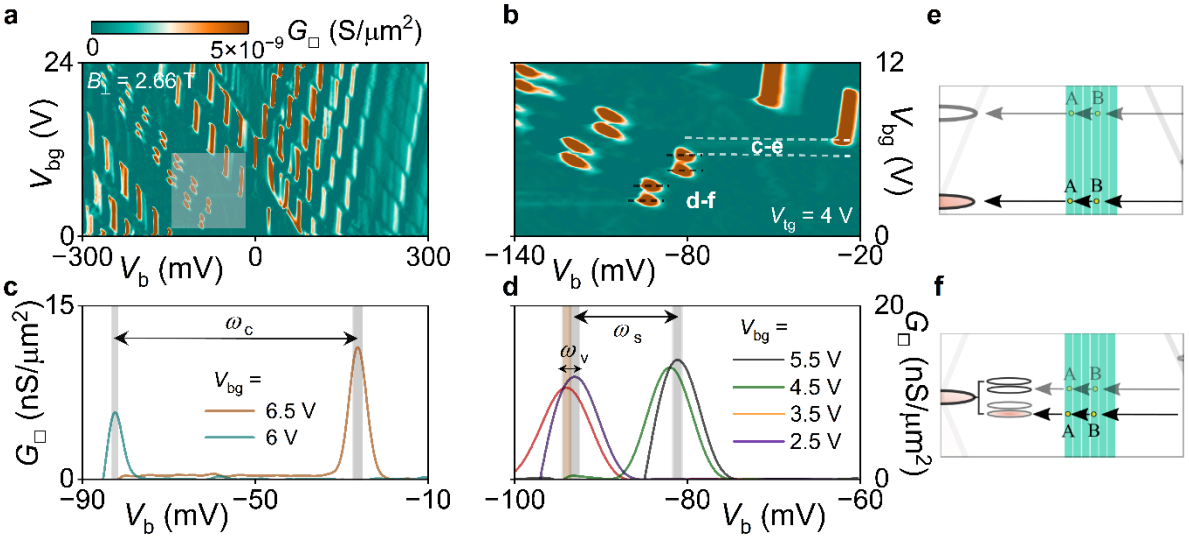

Supplementary Figure 8. Resonant inelastic tunnelling as a tool for the spectroscopy of delicate features in electronic density of states of electrode layers, the case of small magnetic fields. **a,** Experimental differential tunnelling conductance map at $T = 2$ K as a function of bias (V_b) and backgate (V_{bg}) voltages at fixed topgate voltage of 4 V in perpendicular magnetic field of $B = 2.66$ T. Transparent shaded square marks the zoomed region of the map presented in (c). The tunnelling conductance values are normalized over the cross-sectional area of the Device 1 ($S \approx 20\ \mu m^2$). **b,** Zoomed-in section of (a) introducing the alignment of inelastic resonant tunnelling features with the degeneracy lifted zeroth and positive first Landau Levels of monolayer graphene and. **c,** and **d,** Individual cross-sections taken from (b) at backgate voltages of $V_{bg} = 6$ and 6.5 V (c), and $V_{bg} = 2.5, 3.5, 4.5$ and 5.5 V (d) presented to shed light on the spectroscopy of the cyclotron gap of $\omega_c = 50$ meV, between the zeroth and first LLs of monolayer graphene(c), and the degeneracy lifted spin and valley gaps of $\omega_s = 14$ meV and $\omega_v = 2.5$ meV (d). The curves presented in (d) were x2 interpolated with data points for clarity. The curves presented in (c) were smoothed by 150 pts for clarity. **e,** and **f,** Schematic band diagrams illustrate inelastic spectroscopic events through localised states A and B (or B and A) in a series of degeneracy lifted zeroth (d) and positive first (c) Landau Levels of moiré monolayer graphene.

References

1. S. Datta. Quantum Transport: Atom to Transistor. Cambridge University Press (2005).
2. L. Britnell, *et al.*, Electron tunnelling through ultrathin boron nitride crystalline barriers. Nano Letters, Volume 12, Issue 3, Pages 1707-1710 (2012).